BIOCHEMISTRY
including biophysical chemistry & molecular biology

Article

pubs.acs.org/biochemistry

Deciphering the Substrate Specificity of SbnA, the Enzyme Catalyzing the First Step in Staphyloferrin B Biosynthesis

Marek J. Kobylarz,[†] Jason C. Grigg,[†] Yunan Liu,[†] Mathew S. F. Lee,[†] David E. Heinrichs,[‡,§] and Michael E. P. Murphy*[,†]

[†]Department of Microbiology and Immunology, Life Sciences Institute, The University of British Columbia, Vancouver, British Columbia, Canada V6T 1Z3

[‡]Department of Microbiology and Immunology and [§]The Centre for Human Immunology, The University of Western Ontario, London, Ontario, Canada N6A 5C1

Supporting Information

ABSTRACT: *Staphylococcus aureus* assembles the siderophore, staphyloferrin B, from L-2,3-diaminopropionic acid (L-Dap), α-ketoglutarate, and citrate. Recently, SbnA and SbnB were shown to produce L-Dap and α-ketoglutarate from *O*-phospho-L-serine (OPS) and L-glutamate. SbnA is a pyridoxal 5′-phosphate (PLP)-dependent enzyme with homology to *O*-acetyl-L-serine sulfhydrylases; however, SbnA utilizes OPS instead of *O*-acetyl-L-serine (OAS), and L-glutamate serves as a nitrogen donor instead of a sulfide. In this work, we examined how SbnA dictates substrate specificity for OPS and L-glutamate using a combination of X-ray crystallography, enzyme kinetics, and site-directed mutagenesis. Analysis of SbnA crystals incubated with OPS revealed the structure of the PLP-α-aminoacrylate intermediate. Formation of the intermediate induced closure of the active site pocket by narrowing the channel leading to the active site and forming a second substrate binding pocket that likely binds L-glutamate. Three active site residues were identified: Arg132, Tyr152, Ser185 that were essential for OPS recognition and turnover. The Y152F/S185G SbnA double mutant was completely inactive, and its crystal structure revealed that the mutations induced a closed form of the enzyme in the absence of the α-aminoacrylate intermediate. Lastly, L-cysteine was shown to be a competitive inhibitor of SbnA by forming a nonproductive external aldimine with the PLP cofactor. These results suggest a regulatory link between siderophore and L-cysteine biosynthesis, revealing a potential mechanism to reduce iron uptake under oxidative stress.

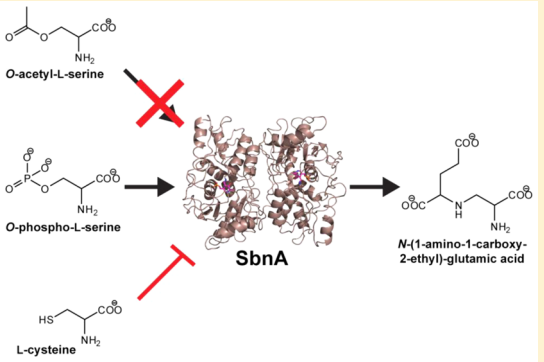

Iron is a limiting nutrient required by most organisms for survival, including the human pathogen *Staphylococcus aureus*.[1] Iron is reactive in aerobic environments, so tight regulatory networks control iron utilization and shuttling throughout the human body.[2] Transport is mediated by host proteins such as transferrin, lactoferrin, haptoglobin, and hemopexin, which also restrict iron availability to microbial pathogens as a form of innate immunity.[3] *S. aureus* overcomes host iron sequestration by using multiple iron uptake strategies including siderophores, low molecular weight, high affinity, ferric iron chelators that scavenge iron from the extracellular environment.[4,5] Ferric iron-bound siderophores are then recognized and imported across the cell membrane by specific transporters. Under iron deprivation, *S. aureus* synthesizes two carboxylate-type siderophores called staphyloferrin A (SA)[6] and staphyloferrin B (SB).[7] The genes responsible for both SA and SB synthesis and transport have been identified and functionally characterized.[8−11] Interestingly, SA-deficient *S. aureus* grows normally in mammalian serum, whereas SB-deficient *S. aureus* growth is attenuated during the exponential phase.[9,12] Furthermore, inactivation of the SB biosynthetic gene cluster impaired *S. aureus* virulence in a mouse infection model[11] and rat infective endocarditis model.[13]

SB is produced by enzymes encoded in the *sbn* gene cluster (*sbnA-sbnI*).[11] Three synthetases (SbnC, E, and F) and a decarboxylase (SbnH) assemble SB from one molecule each of citrate and α-ketoglutarate and two molecules of L-2,3-diamopropionic acid (L-Dap).[10] In addition to the core siderophore assembly proteins, the *sbn* gene cluster also encodes three enzymes that synthesize the essential SB precursors. SbnG is a structurally distinct type of citrate synthase that produces citrate from oxaloacetate and acetyl-CoA.[14,15] Recently, SbnA and SbnB were shown to generate L-Dap and α-ketoglutarate from *O*-phospho-L-serine (OPS) and L-glutamate.[16,17] OPS and L-glutamate can be made available for SB production from the L-serine and L-glutamate biosynthesis pathways, respectively, and these are likely to be abundant substrates when *S. aureus* is in human serum.[18] In this two-step

Received: September 22, 2015
Revised: January 15, 2016
Published: January 21, 2016

DOI: 10.1021/acs.biochem.5b01045
Biochemistry 2016, 55, 927−939

Scheme 1. Proposed Reaction Mechanism for OASS Enzymes and SbnA[a]

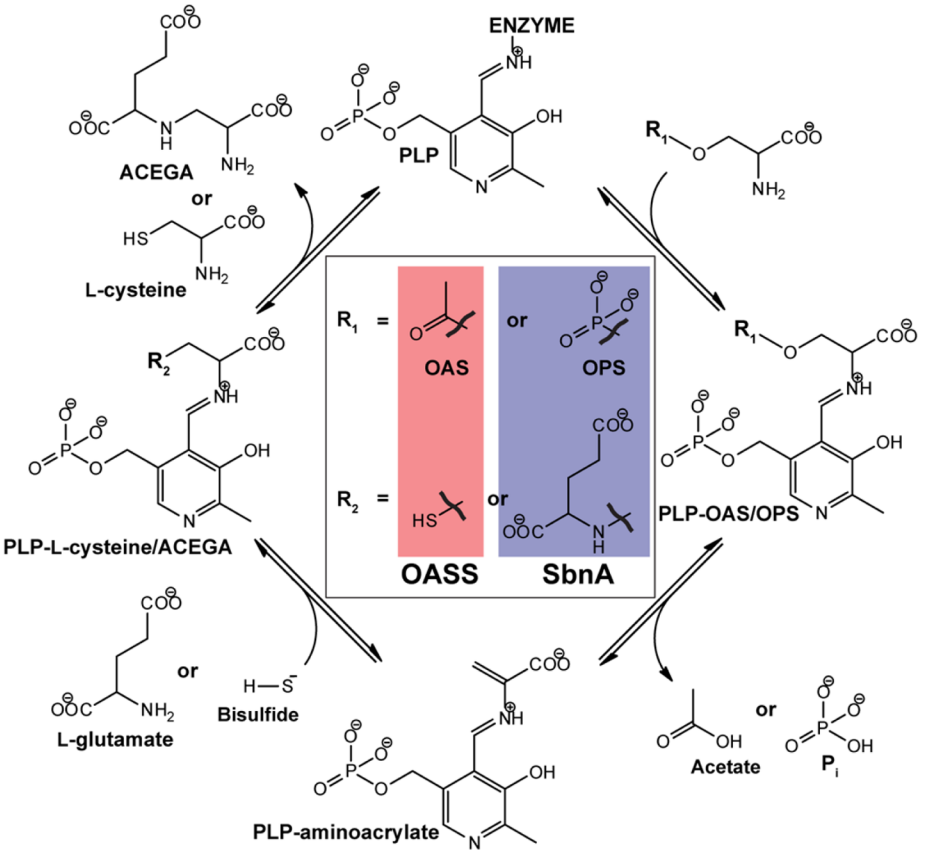

[a]PLP, pyridoxal 5′-phosphate; OAS, *O*-acetyl-L-serine OPS; *O*-phospho-L-serine; ACEGA, *N*-(1-amino-1-carboxy-2-ethyl)-glutamic acid.

biosynthetic pathway, SbnA generates a metabolite called *N*-(1-amino-1-carboxy-2-ethyl)-glutamic acid (ACEGA) from OPS and L-glutamate, while releasing an inorganic phosphate. ACEGA is then oxidatively hydrolyzed by SbnB with NAD^+ to produce L-Dap, α-ketoglutarate, and NADH.

SbnA is a pyridoxal 5′-phosphate (PLP) containing enzyme[17] with homology to the *O*-acetyl-L-serine (OAS) sulfhydrylases (OASS), also commonly annotated as L-cysteine synthases.[16] SbnA homologues are present in other organisms that are predicted to produce SB[16] or structurally similar secondary metabolites, including the antibiotics zwittermicin A,[19] viomycin,[20] capreomycin,[21] and dapdiamide.[22] OASS catalyzes the formation of a PLP-α-aminoacrylate intermediate from OAS with release of acetate (Scheme 1).[23−27] Additionally, a subset of previously annotated OASS enzymes has been discovered to utilize OPS as a substrate instead of OAS. The first identified OPS sulfhydrylase (OPSS) was from a hyperthermophile archaea *Aeropyrum pernix* K1, which catalyzed the formation of L-cysteine from OPS and sulfide.[28] Unlike currently characterized OPSS, SbnA utilizes a unique second substrate in L-glutamate instead of a sulfur donor (Scheme 1).[17] Given the similarities to OASS and OPSS enzymes, it is unclear how SbnA specificity for OPS and L-glutamate is achieved.

The aim of this study was to characterize SbnA reactions, including the specificity for OPS. We demonstrated that in SbnA a PLP-α-aminoacrylate intermediate is produced when incubated with OPS, and this activity is mediated by residues Arg132, Tyr152, and Ser185. The intermediate state of SbnA induced a conformation change that formed a putative L-glutamate binding site. Lastly, we identified L-cysteine as a potent competitive inhibitor of SbnA activity. These findings reveal the structural basis for OPS specificity and a potential regulatory link between SB biosynthesis and the oxidative stress response in *S. aureus*.

EXPERIMENTAL PROCEDURES

Site-Directed Mutagenesis. The SbnA coding region was previously cloned from *S. aureus* strain Newman genomic DNA into the pET28a plasmid.[17] Site-directed mutagenesis of pET28a-*sbnA* was performed using a modified multisite whole plasmid PCR technique.[29] Fifty nanograms of plasmid template was incubated with 0.2 mM dNTPs (Fermentas), 3% dimethyl sulfoxide (New England BioLabs), 0.5 mM NAD^+ (Sigma), 0.36 μM 5′-phosphorylated forward primer(s) (Integrated DNA Technologies), 5 U/μL ampligase (Epicentre), and 2 U/μL Phusion (New England BioLabs) in Phusion HF buffer. Mutagenic primers are shown in Table S1. The PCR conditions were 98 °C for 30 s, then 30 cycles of 98 °C (15 s), 55 °C (60 s), 72 °C (30 s/kilobase) and a final extension cycle at 72 °C for 10 min. The PCR products were then digested with *Dpn*I (New England BioLabs) and transformed into *Escherichia coli* BL21(DE3) (Novagen) by electroporation. All mutations were confirmed by DNA sequencing.

Protein Expression and Purification. Cells were inoculated into 2× YT media and grown with shaking at 30 °C to an optical density of ∼0.8. Expression was induced by the addition of 0.3 mM isopropyl β-D-thiogalactopyranoside (Gold Biotechnology) and grown overnight at 25 °C. Cells were

DOI: 10.1021/acs.biochem.5b01045
Biochemistry 2016, 55, 927−939

Table 1. Data Collection and Refinement Statistics

	SbnA-PLP	SbnA-AA	SbnA Y152F	SbnA Y152F/S185G
Data Collection[a]				
wavelength (Å)	0.97952	1.15869	1.12709	1.12709
resolution range (Å)	50.00−1.45 (1.50−1.45)	37.08−1.92 (1.99−1.92)	35.38−1.50 (1.55−1.50)	34.92−1.50 (1.55−1.50)
unit cell dimension (Å)	a = 56.1 b = 115.8 c = 45.1	a = 56.7 b = 117.4 c = 47.8	a = 56.4 b = 116.0 c = 45.5	a = 56.0 b = 115.2 c = 44.7
unique reflections	53071	25069	47648	46567
completeness (%)	97.3 (94.7)	99.5 (93.2)	98.2 (88.9)	98.9 (93.4)
redundancy	5.9 (5.6)	5.9 (5.5)	6.6 (4.6)	6.3 (4.3)
mean $I/\sigma I$	28.1 (3.3)	13.1 (2.6)	18.6 (5.3)	19.66 (4.5)
R_{merge}	0.055 (0.413)	0.082 (0.536)	0.062 (0.208)	0.061 (0.242)
Wilson B-factor (Å^2)	12.4	22.4	12.7	11.2
Refinement				
R_{work} (R_{free})	12.4 (17.5)	17.1 (21.4)	14.8 (18.0)	15.0 (18.1)
no. of water molecules	364	175	351	402
r.m.s.d. bond length (Å)	0.012	0.013	0.014	0.009
Average B-values (Å^2)				
overall	18.8	28.2	18.1	14.8
protein	16.9	27.6	16.5	13.1
ligands	12.9	41.3	21.4	11.5
water	32.7	35.3	29.8	25.9
Ramachandran plot (%):				
in most-favorable	97.0	97.0	96.0	98.0
in disallowed	0.59	0.0	0.0	0.0
PDB accession code	5D84	5D85	5D86	5D87

[a]Data collection statistics in brackets represents highest resolution shell.

pelleted and lysed in 50 mM Tris (Fisher Scientific) pH 8.0, 100 mM NaCl (Fisher Scientific) using an EmulsiFlex-C5 homogenizer (Avestin). Cell debris was removed by centrifugation and 6x-His tagged protein was purified by Ni^{2+} affinity chromatography using a HisTrap HP column (GE Healthcare). His-tagged SbnA was dialyzed into 50 mM Tris pH 8.0, 100 mM NaCl and digested with thrombin (Haematologic Technologies) for ∼3 h at room temperature. The protein was then passed again through a Ni^{2+}-loaded HisTrap HP column to collect cleaved SbnA in the flow through. Protein samples were >98% pure, as estimated by SDS-PAGE. Modifications to the purification protocol were made to improve stability of protein samples used to determine the SbnA α-aminoacrylate (SbnA-AA) structure and for spectroscopic assays, as follows. All buffer solutions were supplemented with 2 mM Tris(2-carboxyethyl)phosphine (TCEP) (Gold Biotechnology). 6x-His-tag cleavage by thrombin digestion was performed overnight at 4 °C while dialyzing into 50 mM Tris pH 8.0, 100 mM NaCl, and 2 mM TCEP. Cleaved protein was dialyzed for ∼2 h into 50 mM Tris pH 8.0, 2 mM TCEP and was purified using a Source 15Q column (GE Healthcare) equilibrated in the same buffer and eluted with a linear NaCl gradient to 500 mM. Finally, purified samples were dialyzed into 50 mM Tris pH 8.0, 100 mM KCl (Sigma), and 2 mM TCEP. All SbnA variants were prepared in an identical manner. All protein preparations were concentrated to ∼20 mg/mL and stored at −80 °C.

Crystallization. SbnA was dialyzed into 20 mM Tris pH 8.0 and concentrated to ∼20 mg/mL for crystallization. Crystals were optimized by hanging drop vapor diffusion in 2 μL drops containing 1 μL protein solution and 1 μL of 0.1 M Tris pH 8.5, 0.2 M $MgCl_2$ (Sigma), 20−25% polyethylene glycol (PEG) 3350 (Sigma). SbnA crystals were soaked for ∼1 min in mother liquor supplemented with 16% glycerol (Sigma) and flash frozen in liquid nitrogen. SbnA prepared with 2 mM TCEP for substrate soaking experiments was concentrated to ∼20 mg/mL for crystallization and optimized by sitting drop vapor diffusion. Each drop contained 2 μL of protein solution mixed with 2 μL of 0.9−1.1 M sodium citrate (Sigma) pH 6.5. SbnA crystals were further optimized by seeding drops with 0.4 μL of serially diluted crushed crystals in the same solution. Crystals were soaked with 10 mM OPS (Sigma) for ∼30 min followed by a brief soak in mother liquor supplemented with 30% glycerol and flash frozen in liquid nitrogen. Crystals of SbnA variants Y152F and Y152F/S185G were grown by sitting drop diffusion with drops containing 1 μL of protein solution and 1 μL of 0.2 M $MgCl_2$, 0.1 M Tris pH 8.5 and 29−33% PEG 4000 (Sigma). Crystals were briefly soaked in mother liquor supplemented with 30% glycerol and flash frozen in liquid nitrogen.

Data Collection and Structure Solution. Diffraction data for the SbnA-PLP complex were collected on beamline 08B1-1 at the Canadian Light Source. Data were processed using HKL2000.[30] The crystals grew in the space group $P2_12_12$ with one molecule in the asymmetric unit. The molecular replacement search model was generated in the program Sculptor[31] from the Phenix program suite[32] using the *Thermatoga maritima* OASS structure (PDB ID: 1O58, 37% identity over 295 of 326 amino acids). The search model excluded the first two histidine residues, loop residues 186, 193 and contained several conservative mutations in surface residues to minimize differences in side chain conformers. Molecular replacement phases were obtained using Phaser-MR,[33] and an initial model of SbnA-PLP was built using

DOI: 10.1021/acs.biochem.5b01045
Biochemistry 2016, 55, 927−939

Autobuild[34] The structure was manually built with Coot[35] and refined with Refmac[36] from the CCP4 program suite.[37] Diffraction data for SbnA-AA and the SbnA variants Y152F and Y152F/S185G were collected at Stanford Synchrotron Radiation Light Source on beamline 7-1. SbnA-AA data were integrated and scaled using XDS[38,39] and phased using Phaser-MR. SbnA Y152F and Y152F/S185G were integrated with Mosflm[40] and scaled with Scala[41] from the CCP4 program suite.[37] SbnA-AA, Y152F, and Y152F/S185G were manually built using Coot[35] and refined using phenix.refine[42] with 6, 4, and 5 translation libration screw (TLS) groups, respectively.[43] Data collection and refinement statistics are provided in Table 1.

Determination of Oligomeric State in Solution. SbnA was dialyzed into 50 mM Tris pH 8.0, 200 mM NaCl. SbnA solutions were concentrated to 0.5 mg/mL and analyzed by dynamic light scattering using a Wyatt DynaPro plate reader (Wyatt Technologies). Data represent the average of five readings from three samples. SbnA was also analyzed by size exclusion chromatography coupled with multiangular light scattering. SbnA was concentrated to 5 mg/mL in 50 mM Tris pH 8.0, 100 mM KCl, and 2 mM TCEP and 100 μL was injected into a HPLC 1260 Infinity LC (Agilent Technologies) attached to a Superdex 200 10/300 column (GE Healthcare) with a flow rate of 0.2 mL/min. Data were collected using a miniDAWN TREOS multiangle static light scattering device and an Optilab T-rEX refractive index detector (Wyatt Technologies). Analysis was performed using the ASTRA6 program (Wyatt Technologies).

Enzyme Assays and Steady-State Kinetics. Formation of the PLP-α-aminoacrylate was monitored by UV−visible spectroscopy. Spectra were measured with 20 μM wild type SbnA or SbnA variants in 50 mM Tris pH 8.0 and 2 mM TCEP with a Varian Cary 50 UV−vis spectrophotometer at room temperature. Spectra were recorded after the addition of 50 μM OPS or 1 mM L-cysteine (Sigma) and incubated for 5 min. The spectrum of 50 μM PLP in the presence of 1 mM L-cysteine in 50 mM Tris pH 8.0 and 2 mM TCEP was recorded every 5 min for 20 min total.

Production of ACEGA, the product of the SbnA reaction, was measured using a coupled assay with SbnB. NADH generation was monitored by absorbance at 340 nm for 10 min at room temperature on a Varian Cary 50 UV−vis spectrophotometer. Coupled reactions contained 50 mM Tris pH 8.0, 100 mM KCl, 2 mM TCEP, 10 μM SbnA, 10 μM SbnB, 1 mM OPS, 1 mM L-glutamate (Sigma), and 100 μM NAD^+. All reactions were performed in triplicate. The extinction coefficient 6220 M^{-1} cm^{-1} was used to quantify the amount of NADH generated.

SbnA enzymatic activity was also measured by monitoring inorganic phosphate release from OPS using a coupled enzymatic assay, as previously described.[44] All data were collected on a Varian Cary 60 UV−vis spectrophotometer with a Varian Cary Single Cell Peltier temperature block set to 25 °C. The reaction mixture contained: 100 nM wild type SbnA or S185G in 50 mM Tris pH 8.0, 2 mM TCEP, 1 U purine nucleoside phosphorylase, and 200 μM 2-amino-6-mercapto-7-methylpurine riboside. Also, the concentrations of OPS (0.005−10.0 mM) or L-glutamate (0.1−100 mM) were varied in the coupled enzymatic assay reaction mixtures. The absorbance increase at 360 nm was recorded every 0.1 s for 120 s, capturing the linear range of activity. The concentration of inorganic phosphate released from OPS was determined using the extinction coefficient of 11 000 M^{-1} cm^{-1}.[44] Data were fit by nonlinear regression analysis using a Michaelis−Menten model in Graphpad Prism 6. The inhibition constant (K_i) for L-cysteine was also determined using the inorganic phosphate assay. 10 nM wild type SbnA or 100 nM S185G were used in 50 mM Tris pH 8.0 and 2 mM TCEP. OPS (0.05−10 mM) dependence was measured at various L-cysteine concentrations (0−10 mM). The K_i was determined with Graphpad Prism 6 using a competitive inhibition model as described by eqs 1 and 2.

$$K_{M_{obs}} = K_M\left(1 + \frac{[I]}{K_i}\right) \quad (1)$$

$$V_o = \frac{v_{max}[S]}{K_{M_{obs}} + [S]} \quad (2)$$

Stopped-Flow Analysis. Data were collected from an SX.18MV stopped-flow reaction analyzer (Applied Photophysics) using a 4.96 nm/mm bandpass monochromator with the slit width set at 0.5 mm. The flow cell temperature was maintained at 25 ± 1 °C. A photodiode array detector was used to collect single wavelength measurements. 10 μM wild type and variant SbnA in 50 mM Tris pH 8.0 and 2 mM TCEP were mixed with varying concentrations of OPS and L-cysteine. PLP-aminoacrylate formation was measured at 467 nm and PLP binding to L-cysteine was measured at 412 nm. Data were collected in triplicate with 1000 data points collected over 2 s. Both the formation of the aminoacrylate intermediate and decay of the internal Schiff base due to L-cysteine binding were fit to single phase exponential functions described by eq 3, where A_t is the absorbance at time t, A_∞ is the absorbance at time ∞, A_i is the amplitude of the ith transient, and k_i is the observed first-order rate constant (k_{obs}) for the ith transient.

$$A_t = A_\infty \pm \sum_i A_i e^{-k_i t} \quad (3)$$

All observed rates were plotted as a function of either OPS or L-cysteine concentration. In the case of OPS, a hyperbolic function was fit to the data. Data for L-cysteine were fit by a linear function. Rate constants were calculated using a rapid equilibrium binding model (eq 4), as previously described for *O*-phospho-L-serine sulfhydrylase (OPSS) enzymes,[45] where $K_1 = 1/K_d$, [S] is the substrate concentration and k_2 is the observed rate of the PLP-aminoacrylate formation. The reverse observed reaction rate (k_{-2}) is assumed to be negligible under the experimental conditions.

$$k_{obs} = \frac{k_2 K_1[S]}{K_1[S] + 1} + k_{-2} \quad (4)$$

Bioinformatic Analysis. A subset of SbnA homologues predicted to be involved L-Dap biosynthesis were chosen from sequence alignments previously performed by Beasley et al. 2011.[16] Another subset of biochemically validated and structurally characterized OASS and OPSS enzymes were identified by a primary sequence search in the Protein Data Bank using the BLAST method with an *E*-value cutoff of 10.0 and had sequence identities over 30%. Additionally, the OPSS enzyme CysO from *Aeropyrum pernix* was included even though its sequence identity was 23%. Also included was the closest *S. aureus* homologue, the OASS CysK and a third recently biochemically validated OPSS enzyme, CysK2, from

DOI: 10.1021/acs.biochem.5b01045
Biochemistry 2016, 55, 927−939

M. tuberculosis. Multiple sequence alignments were generated on the EMBL-EBI Web site using Clustal Omega set to default parameters.[46]

RESULTS

Structure of SbnA. SbnA crystallized with a single molecule in the asymmetric unit, containing two mixed α/β domains. Each domain was made up of a central β-sheet surrounded by several α-helices with a single PLP bound within a central cavity between the domains (Figure 1A). The overall fold places SbnA in the Class II PLP-dependent enzyme family.[47] Size exclusion chromatography in line with multiangle light scattering demonstrated that SbnA (36 kDa monomer) forms a dimer in solution with mass of 77 kDa (Figure S1). A similar mass of 82 kDa was determined by dynamic light scattering (data not shown). The biological SbnA dimer could be reconstructed across the 2-fold crystallographic symmetry axis (Figure 1B). The dimer interface was contributed by ~50 residues, burying ~1800 Å^2 of surface area from solvent (8% of total surface area) in each monomer, as determined using the program PISA.[48]

The active site is in a large cleft lined by positively charged residues from one monomer, and both active sites are accessible from same face of the dimer (Figure 1B). PLP copurified with the enzyme and was observed covalently bound to Lys47 at the base of the cleft by an internal Schiff base originating from the PLP *si* face (Figure 1C). The structure of the as-isolated enzyme is referred to as SbnA-PLP. The PLP phosphate formed hydrogen bonds to Ser185, Thr186, Thr187, and Ser189 and three water molecules (Figure 1C). The negative charge on the phosphate was stabilized by the positive helix dipole of the α-helix spanning residues 188−200. The pyridoxal portion formed hydrogen bonds with Asn77 and Ser272 (Figure 1C). The *re* face PLP pyridine ring is exposed to solvent providing access for substrate to displace the lysine Schiff base at C4′ to form an external aldimine.

SbnA Forms a PLP-α-aminoacrylate Intermediate with OPS. OPS was previously shown to be a substrate of SbnA.[17] Soaking OPS into SbnA crystals resulted in an observable color change from pale to golden yellow, mirroring the absorption changes previously observed in solution,[17] suggesting that a PLP-α-aminoacrylate intermediate formed in the crystals. The OPS-soaked SbnA crystal structure (SbnA-AA) was solved to 1.92 Å resolution. In the SbnA-AA structure, clear electron density for the PLP-α-aminoacrylate was observed and could be modeled and refined at full occupancy with an average *B*-factor of 24 Å^2 (Figure 2A). Electron density corresponding to the OPS phosphate group was not observed. The covalent bond formed between Lys47 and the PLP cofactor in the SbnA-PLP structure is displaced by formation of the PLP-α-aminoacrylate. Instead, the side chain amine of Lys47 replaced a water molecule to form a new hydrogen bond with the PLP phosphate (Figure 1C and Figure 2B). Overlaying the SbnA-PLP and SbnA-AA structures (root-mean-square deviation (rmsd) of 1.1 Å over all C_α atoms) revealed that the C-terminal domain has rotated toward the N-terminal domain narrowing the active site cleft (Figure 2C). Within the active site, the pyridoxal ring of the PLP-α-aminoacrylate is rotated approximately 20° with respect to SbnA-PLP (Figure 2D). This rotation repositions the α-aminoacrylate carboxylic acid to form hydrogen bonds to Thr74, Ser75, Leu78, and Gln151 (Figure 2B). In concert, the active site loop (residues 72−76), which contains a highly conserved serine (Ser75), is translated up to ~4 Å bringing it directly above the α-aminoacrylate (Figure 2C).

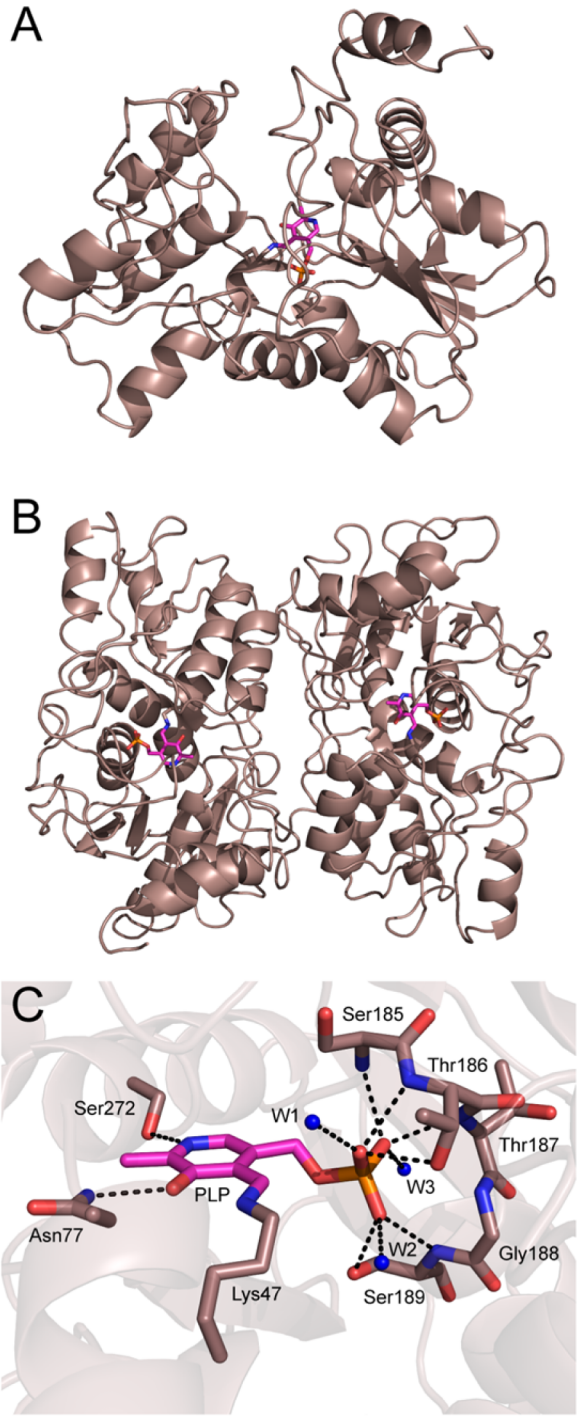

Figure 1. Structure of SbnA. (A) The overall fold of SbnA is shown as a cartoon. The PLP cofactor, colored magenta, is shown in stick form in the active site cleft. (B) The SbnA dimer reconstructed by applying 2-fold crystallography symmetry. (C) The active site of SbnA with PLP interacting residues shown as sticks. Ordered water molecules are shown as blue spheres and the dashed lines represent potential hydrogen bonds. C, N, O, P atoms are colored brown, blue, red, and orange, respectively with PLP carbons colored magenta.

A second binding pocket is formed between the two domains directly above the PLP-α-aminoacrylate. Citrate was present in the crystallization condition, and electron density for a citrate molecule was identified in the newly formed pocket. Citrate

DOI: 10.1021/acs.biochem.5b01045
Biochemistry 2016, 55, 927−939

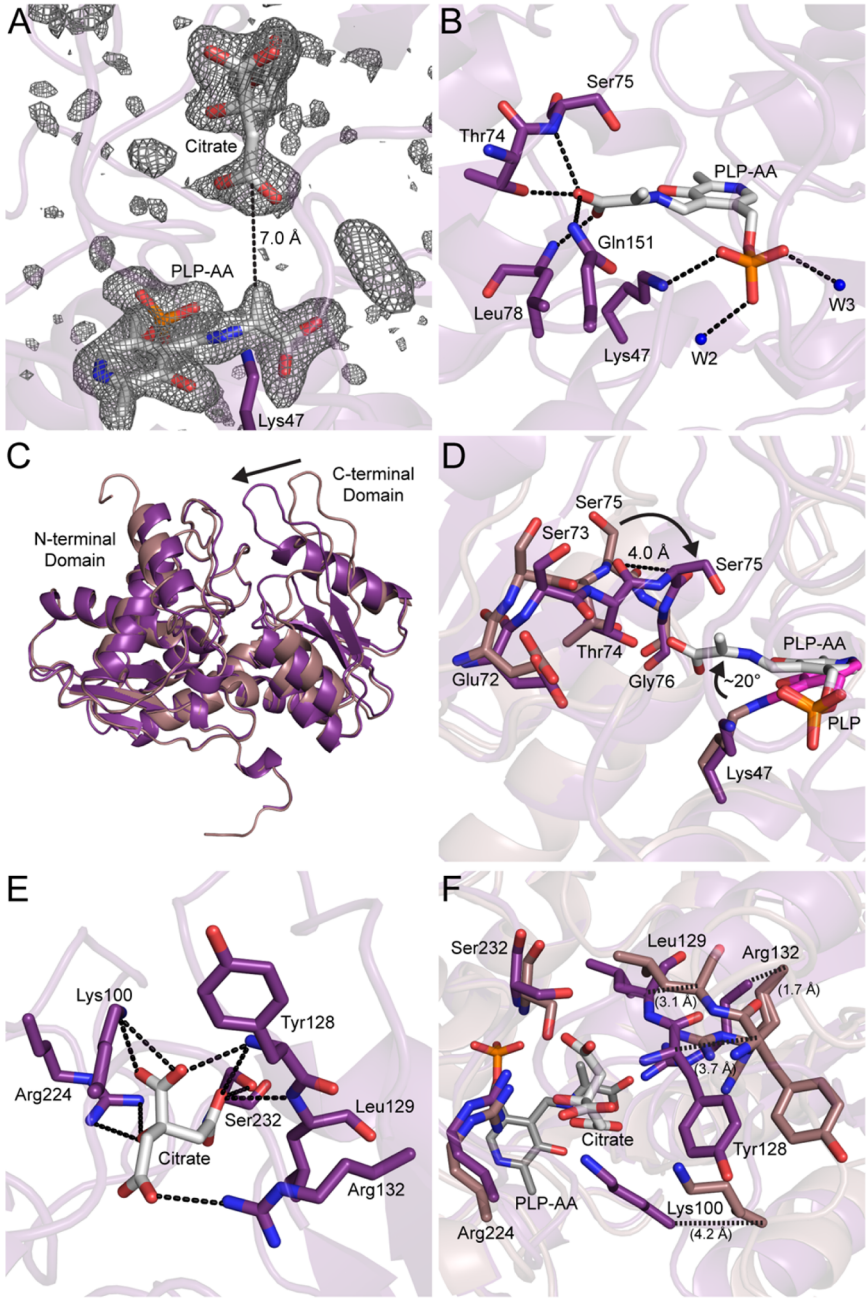

Figure 2. SbnA adopts a closed conformation when bound to the PLP-α-aminoacrylate. (A) The active site of SbnA-AA contains the PLP-α-aminoacrylate intermediate and a citrate molecule. Both molecules are shown as sticks and colored white. The dashed line represents the distance between the α-aminoacrylate β-carbon and citrate. Omit difference ($F_0 - F_c$) electron density is shown as a gray mesh contoured to 3.0 σ. (B) The SbnA active site with the PLP-α-aminoacrylate intermediate binding residues shown as sticks. Ordered water molecules are shown as blue spheres, and the dashed lines represent hydrogen bonds. (C) The overall structural overlay of SbnA-PLP (brown) and SbnA-AA (purple) as shown in cartoon reveals significant conformational changes in the C-terminal domain. The black arrow highlights directionality of the conformational change upon PLP-α-aminoacrylate formation. (D) Structural overlay of SbnA-PLP (brown) and SbnA-AA (purple) active sites reveal a significant conformational change in the loop containing residue Ser75. The dashed line indicated the distance between C_α atoms of Ser75 upon α-aminoacrylate formation and the curved black arrows represent the conformational shift for PLP and Ser75. (E) Citrate binds into a newly identified pocket above the active site in the SbnA-AA structure. Citrate (white) and bonding residues are shown as sticks, and the dashed lines represent hydrogen bonds. (F) Structural overlay of SbnA-PLP (brown) and SbnA-AA (purple) citrate binding sites. The dashed lines indicate the distances between the C_α atoms of Lys100, Tyr128, Leu129, and Arg132 upon α-aminoacrylate formation. The citrate (white) and PLP-α-aminoacrylate (dark gray) are shown as sticks.

was modeled and refined at full occupancy with an average *B*-factor of 34 Å^2 (Figure 2A). The citrate molecule was bound by an extensive hydrogen bonding network mediated by the positively charged side chains from Lys100, Arg132, and Arg224 as well as the backbone chain amide groups of Tyr128, Leu129, and Ser232 (Figure 2E). An overlay between SbnA-PLP and SbnA-AA revealed a significant conformational change that formed a second binding pocket. The C_α atoms of residues forming the citrate binding site (Lys100, Tyr128, Leu129, and Arg132) were displaced by more than 1.7 Å (Figure 2F). The

DOI: 10.1021/acs.biochem.5b01045
Biochemistry 2016, 55, 927−939

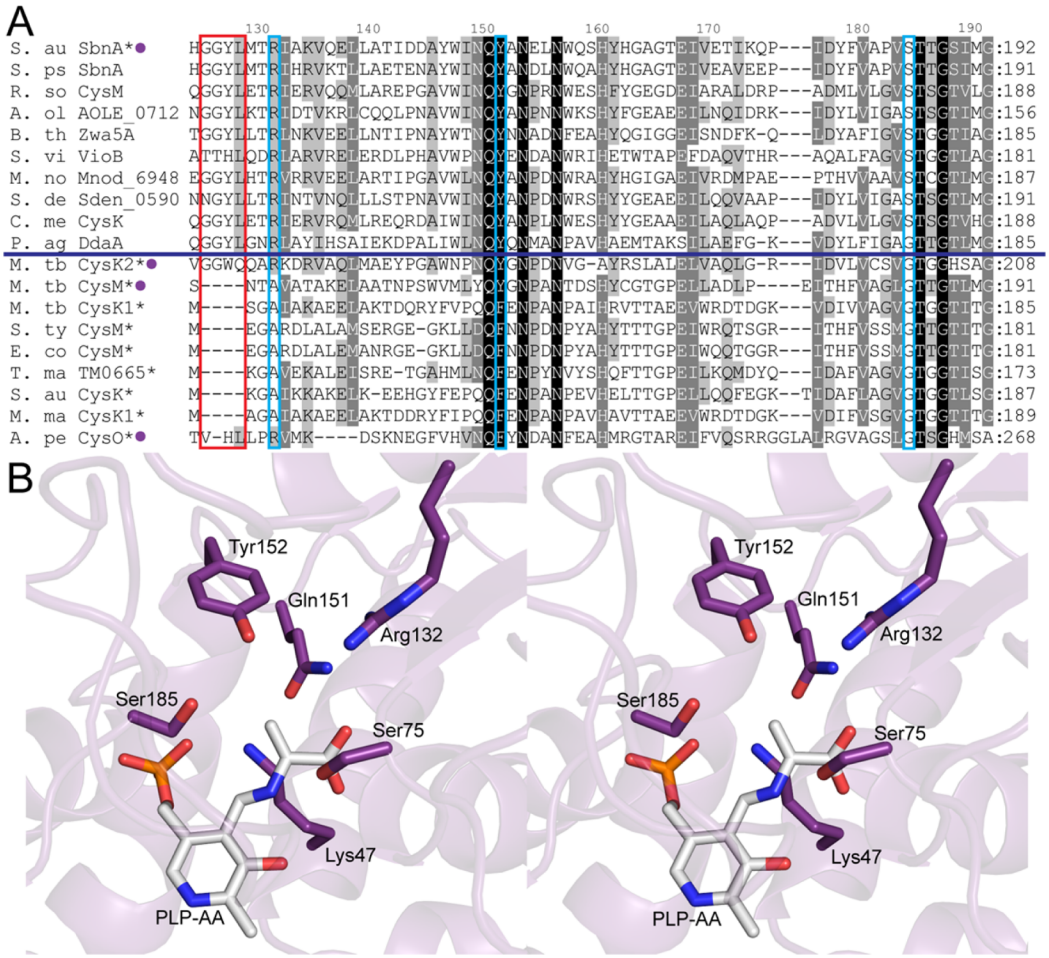

Figure 3. Identification of OPS discriminating residues. (A) Multiple sequence alignment of SbnA and homologous sequences found in the tryptophan synthase beta superfamily. Sequences are identified by a single letter for genus, the first two letters of the species name and the annotated protein name. The asterisk placed after the protein name(s) indicates biochemically validated OASS or OPSS enzymes, and the purple circles represent experimentally validated OPS utilizing enzymes. The dark blue line represents the divide between SbnA homologues likely involved in L-Dap synthesis and other OASS and OPSS enzymes. Conserved active site residues between OASS and OPSS enzymes are highlighted in blue boxes. A four amino acid insert identified in SbnA homologues that are responsible for L-Dap synthesis is highlighted in a red box. Numbering along the top corresponds to the sequence position of *S. aureus* SbnA. S. au, *Staphylococcus aureus*; S. ps, *Staphylococcus pseudintermedius*; R. so, *Ralstonia solanacearum*; A. ol, *Acinetobacter oleivorans*; B. th, *Bacillus thuringiensis*; S. vi, *Streptomyces vinaceus*; M. no, *Methylobacterium nodulans*; S. de, *Shewanella denitrificans*; C. me, *Cupriavidus metallidurans*; P. ag, *Pantoea agglomerans*; M. tb, *Mycobacterium tuberculosis*; S. ty, *Salmonella typhimurium*; E. co, *Escherichia coli*; T. ma, *Thermotoga maritime*; M. ma, *Mycobacterium marinum*; A. pe, *Aeropyrum pernix*. (B) Stereo view of the SbnA-AA active site highlighting residues implicated in OPS selectivity. PLP-AA and residues are shown as sticks.

β-carbon of the α-aminoacrylate was approximately 7.0 Å from the C_α carboxylate moiety of the citrate (Figure 2A).

SbnA Active Site Variants. Despite sharing homology with OASS enzymes, no activity was detected for SbnA using OAS as a substrate.[17] To identify residues that could provide specificity for OPS, a multiple sequence alignment was constructed to include homologues from other siderophore or antibiotic biosynthetic gene clusters, as well as characterized OPSS and OASS enzymes. The multiple sequence alignment revealed three residues that are predicted to be associated with L-Dap synthesis, Arg132, Tyr152, and Ser185, due to their conservation in SbnA and homologues in gene clusters with a SbnB homologue (Figure 3A). In the SbnA structures, these three residues surround the α-aminoacrylate and could interact with the OPS phosphoryl group (Figure 3B). In contrast, in characterized OAS dependent homologues, positions 132, 152, and 185, are substituted by conserved alanine, phenylalanine, and glycine residues. To determine the role these three residues play as key determinants of OPS versus OAS specificity, four variants were generated: R132A, Y152F, S185G, Y152F/S185G, and evaluated for OPS and OAS dependent activity.

The four variants were tested for the ability to form the PLP-α-aminoacrylate intermediate with either OPS or OAS. Both the Y152F and S185G SbnA retained the ability to form the PLP-α-aminoacrylate intermediate with OPS (Figure S2A,B). In contrast, intermediate formation with OPS was abolished in Y152F/S185G and R132A SbnA (Figure S2C,D). None of the SbnA variants generated formed the intermediate upon the addition of OAS (data not shown).

Kinetic Analysis of SbnA and Variants. Enzyme turnover was monitored in a coupled assay to monitor ACEGA production that contained SbnA, SbnB, OPS, L-glutamate, and NAD^+ in 50 mM Tris pH 8.0, 100 mM KCl, and 2 mM TCEP. Product formation was decreased for all four SbnA variants compared to wild type SbnA (Figure S3). R132A SbnA had no detectable activity, which correlates with absorption spectra that showed this variant did not form the α-aminoacrylate intermediate (Figure S2). L-Dap, a product of

DOI: 10.1021/acs.biochem.5b01045
Biochemistry 2016, 55, 927−939

SbnB, appeared to inhibit the activity of SbnB causing interference in the coupled assay. Thus, SbnA turnover was additionally monitored by a phosphate assay. Optimal wild-type enzyme activity as monitored by phosphate release was observed with no KCl (0−500 mM tested) at pH 8.0 (6.5−8.5 tested) in a 50 mM Tris buffer (Figure S4). KCl likely inhibited enzymatic activity *in vitro* by impeding formation of the quinonoid intermediate, a phenomenon observed in other PLP-dependent enzymes.[49,50] Therefore, KCl was removed as a SbnA buffer component in all future experiments. Steady-state kinetics was used to investigate the mechanism of SbnA catalysis. Enzyme rates were measured for wild type SbnA and the S185G variant as a function of OPS and glutamate concentration (Figure S5), and steady-state kinetic parameters are summarized in Table 2. SbnA S185G was the only variant examined because all other variants were insufficiently active to accurately measure enzyme rates (Figure S3). SbnA S185G had a modest decrease in catalytic efficiency of ∼4-fold compared to the wild type enzyme (Table 2).

Table 2. Steady-State Kinetic Parameters of Wild Type SbnA and SbnA S185G[a]

	K_m (mM)	k_{cat} (s^{-1})	k_{cat}/K_m (M^{-1} s^{-1})
OPS			
SbnA WT	0.072 ± 0.008	2.3 ± 0.06	$3.2 \times 10^4 \pm 3.6 \times 10^3$
SbnA S185G	0.22 ± 0.009	1.6 ± 0.02	$7.3 \times 10^3 \pm 3.0 \times 10^2$
L-glutamate			
SbnA WT	3.2 ± 0.2	3.6 ± 0.06	$1.1 \times 10^3 \pm 7.8 \times 10^1$
SbnA S185G	7.1 ± 1.5	2.0 ± 0.1	$2.9 \times 10^2 \pm 6.4 \times 10^1$

[a]All reactions were performed in 50 mM Tris pH 8.0 and 2 mM TCEP. The Michaelis−Menten plots for both OPS and L-glutamate are illustrated in Supplementary Figure S5.

The rate of formation of the PLP-α-aminoacrylate intermediate with OPS was determined for wild type SbnA and the Y152F and S185G variants (Figure S6). The rate of intermediate formation was best fit by a single-exponential function at each concentration of OPS tested, and the dependence of OPS concentration on the apparent first-order rate constants was then best described by hyperbolic functions. Single turnover kinetic parameters for wild type, S185G, and Y152F SbnA are summarized in Table 3. Relative to wild type SbnA, mutating Ser185 to Gly did not greatly impact α-aminoacrylate formation as evidenced by a modest ∼2-fold decrease in the second order rate constant (Table 3). Mutating Tyr152 to Phe resulted in an over 1000-fold decrease in the second order rate constant. These data suggest that Arg132, Tyr152, and Ser185 play a role in OPS binding and formation of the PLP-α-aminoacrylate intermediate, though each contributes to varying degrees.

Table 3. Single Turnover Kinetic Parameters of Wild Type SbnA and SbnA Variants with Various Concentrations of OPS[a]

	k_{obs} (s^{-1})	K_d (mM)	K_2 (M^{-1} s^{-1})
SbnA WT	$3.1 \times 10^2 \pm 1.2 \times 10^1$	2.8 ± 0.2	$1.1 \times 10^5 \pm 1.0 \times 10^4$
SbnA S185G	$1.4 \times 10^2 \pm 6.6 \times 10^1$	3.4 ± 0.4	$4.0 \times 10^4 \pm 5.4 \times 10^3$
SbnA Y152F	1.5 ± 0.06	15 ± 1.7	$1.0 \times 10^2 \pm 1.2 \times 10^1$

[a]All reactions were performed in 50 mM Tris pH 8.0 and 2 mM TCEP. OPS single-turnover plots are illustrated in Supplementary Figure S6.

SbnA Variant Crystal Structures. To characterize the structural alterations of the active sites in Y152F and Y152F/S185G SbnA, X-ray crystal structures were solved to 1.5 Å resolution. Electron density for PLP covalently bound to Lys47 was observed in the active site of both variant structures. The crystal structure of Y152F SbnA displayed minimal conformational change when compared to wild type SbnA (rmsd of 0.11 Å over all C_α atoms) (Figure S7). Since minimal structural changes were observed and Y152 does not interact directly with the PLP-α-aminoacrylate, this residue may interact with the phosphate group of OPS, consistent with a decrease in the rate of intermediate formation. Alternatively, Y152 may mediate the second step in the reaction, the bond formation between the β-carbon of the α-aminoacrylate and the amino group of L-glutamate. In contrast, the Y152F/S185G SbnA structure displayed a greater conformational change when compared to SbnA-PLP (rmsd of 0.34 Å over all C_α atoms) (Figure 4). A significant conformational change was observed within the active site loop (residues 72−76), which is translated toward the PLP cofactor by up to ∼2.5 Å when compared to SbnA-PLP (Figure 4A,B). The conformational change shares some of the features that occurred upon α-aminoacrylate formation in SbnA-AA. Gln151 was rotated ∼40° about χ_2 to mimic the orientation of Gln151 in SbnA-AA that turns in to bind the α-aminoacrylate (Figure 4C). Therefore, SbnA Y152/S185G adopted a similar active site conformation to SbnA-AA, even in the absence of the α-aminoacrylate. These similarities suggest that the double mutant inhibits OPS binding by mimicking the closed active site conformation of the protein, potentially explaining its lack of activity.

L-Cysteine Inhibits SbnA Activity. In addition to OAS and OPS, some SbnA homologues can bind and utilize L-cysteine as a substrate.[45] When L-cysteine was added to wild type SbnA, the characteristic internal aldimine absorption maxima at 412 nm diminished, but no spectral signature at 467 nm for a PLP-α-aminoacrylate intermediate formed (Figure 5). Instead, a subsequent increase at 320 nm was observed suggesting that L-cysteine bound to the PLP cofactor and formed an external aldimine bond by forming a thiazolidine ring between the formyl group of PLP and the amino and sulfhydryl groups of L-cysteine.[51] Mixing L-cysteine with PLP in the absence of SbnA resulted in a similar spectral change, but at a significantly slower rate as only a small decrease at 412 nm and subsequent increase at 320 nm was observed after 20 min (Figure S8). Near complete quenching of PLP was observed after 5 min with SbnA, indicating that SbnA catalyzes the reaction between PLP and L-cysteine. In CysM from *M. tuberculosis*, the reaction with L-cysteine results in the formation of the PLP-α-aminoacrylate and release of bisulfide.[45] The spectra of wild type SbnA implies that a different intermediate is formed that is unable to release bisulfide to form the α-aminoacrylate. The absorption spectra for all four variants demonstrated a similar decrease at 412 nm, though to varying levels, except for R132A, in which the absorption maxima shifted to 467 nm (Figure 5). Competitive inhibition by L-cysteine of wild type SbnA and S185G SbnA activity was characterized by steady-state kinetics (Figure S9). The K_i for L-cysteine was 91 ± 16 μM, while the K_i for L-cysteine against S185G SbnA was 2.1 ± 0.5 mM, a ∼23-fold reduction compared to wild type SbnA. Additionally, the single turnover kinetics for L-cysteine binding to wild type SbnA and variants

DOI: 10.1021/acs.biochem.5b01045
Biochemistry 2016, 55, 927−939

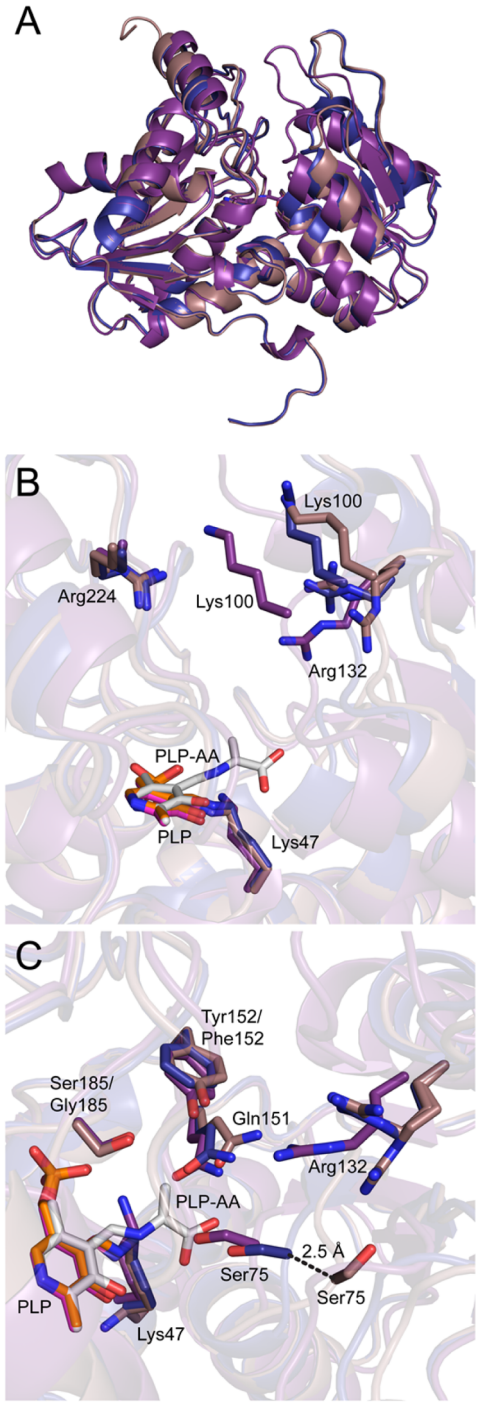

Figure 4. Structure of the SbnA variant Y152F/S185G. Structural overlay of SbnA-PLP (brown), SbnA-AA (purple), and SbnA Y152F/S185G (blue) showing the (A) overall fold, (B) L-glutamate binding pocket, and (C) PLP-AA binding pocket. All ligands and residues are shown as sticks. The dashed line represents the shift between C_α atoms of Ser75 upon OPS binding.

was characterized (Table 4 and Figure S10). In contrast to reaction with OPS, no significant differences in the second order rate constants were observed between wild type SbnA and most variants at physiologically relevant L-cysteine concentrations. However, in Y152F/S185G SbnA reacted with L-cysteine at a 10-fold greater rate than wild type SbnA. The data suggest that reaction with L-cysteine is mediated in a different manner compared to OPS binding and appears to be independent of Arg132, Tyr152, and Ser185.

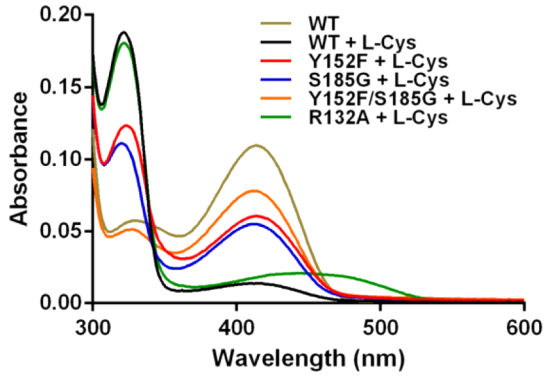

Figure 5. UV−visible absorption spectra of wild type SbnA and SbnA variants with 1 mM L-cysteine. The spectra were recorded at room temperature for 20 μM protein in 50 mM Tris pH 8.0 and 2 mM TCEP.

Table 4. Single Turnover Kinetic Parameters of Wild Type SbnA and SbnA Variants with Various Concentrations of L-Cysteine[a]

	k_{obs} (s^{-1})	K_d (mM)	K_2 (M^{-1} s^{-1})
SbnA WT			$4.0 \times 10^2 \pm 1.2 \times 10^1$
SbnA Y152F			$2.0 \times 10^2 \pm 8.6$
SbnA S185G			$7.1 \times 10^2 \pm 4.6 \times 10^1$
SbnA Y152F/S185G	18 ± 3.7	8.9 ± 3.2	$2.0 \times 10^3 \pm 8.5 \times 10^2$
SbnA R132A			$4.4 \times 10^2 \pm 1.7 \times 10^1$

[a]All reactions were performed in 50 mM Tris pH 8.0 and 2 mM TCEP. L-Cysteine single-turnover plots are illustrated in Supplementary Figure S10.

DISCUSSION

We recently elucidated the L-Dap biosynthetic pathway required for SB biosynthesis in *S. aureus*.[17] In this pathway, SbnA generates the novel serine-glutamate conjugate, ACEGA, from OPS and L-glutamate. SbnB then oxidatively hydrolyzes ACEGA to generate L-Dap and α-ketoglutarate.[17] Sequence homology places SbnA in the tryptophan synthase beta superfamily, which are all PLP-dependent enzymes. Among the biochemically characterized members of this superfamily, SbnA is most similar in sequence to OASS enzymes involved in L-cysteine biosynthesis. SbnA was hypothesized to produce L-Dap from OAS and an ammonium ion liberated from SbnB.[16] However, SbnA falls into a small subclass of OASS-like enzymes that instead utilize OPS as a substrate. Unlike most characterized OASS/OPSS enzymes, SbnA uses a nitrogen donor rather than a sulfur donor such as bisulfide.[17]

An ~100-fold difference in K_m values of SbnA for OPS and L-glutamate was observed and may reflect the relative abundance of each metabolite in *S. aureus* under iron deprivation. In *S. aureus*, L-glutamate is one of the most abundant amino acids with intracellular concentrations exceeding 100 mM in some growth conditions,[52,53] sufficient to saturate SbnA. The intracellular OPS concentration has not been determined in *S. aureus*. On the basis of KEGG pathways,[54,55] the main route for L-serine biosynthesis is derived from glycolysis via OPS by the enzymes SerABC. The micromolar K_m for OPS may reflect the low intracellular OPS concentrations in *S. aureus*. How the intracellular concentration of OPS and other amino acids

DOI: 10.1021/acs.biochem.5b01045
Biochemistry 2016, 55, 927−939

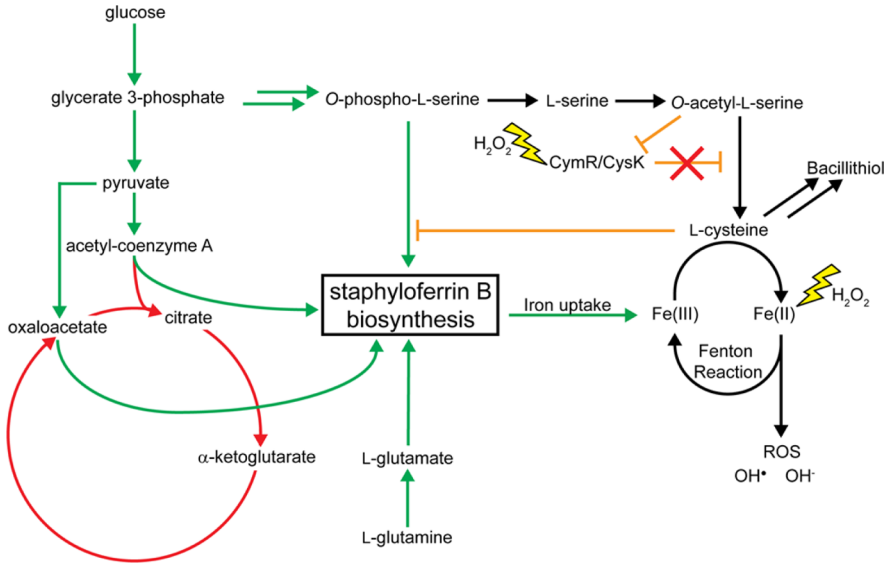

Figure 6. Proposed flow diagram of staphyloferrin B biosynthesis integrated into primary metabolism of *S. aureus* under nutrient deprivation and oxidative stress. Green arrows represent upregulated metabolic pathways; red arrows indicate downregulated metabolic pathways and black arrows represent unchanged metabolic pathways. Orange, blunt ended lines represent inhibition pathways. ROS stands for reactive oxygen species.

including L-glutamate changes under iron deprivation remains to be determined.

Superposition of SbnA-PLP and SbnA-AA revealed the enzyme undergoes significant conformational changes. Similar collapsing of the active site upon PLP-α-aminoacrylate intermediate formation is observed in structures determined for homologues CysK1 and CysM from *M. tuberculosis*.[25,56] Loss of the phosphate group upon formation of the stable PLP-α-aminoacrylate intermediate from OPS precluded direct structural identification of residues involved in OPS specificity. However, the active site of SbnA-AA revealed three residues: Arg132, Tyr152, and Ser185 are in close proximity to the β-carbon of the α-aminoacrylate intermediate (Figure 3B), and all three residues were shown to be involved in formation of the intermediate. Sequence divergence in these active site residues from OASS enzymes likely allows SbnA to bind OPS with high specificity. We hypothesized that mutating the active site of SbnA to mimic active sites of OASS enzymes could shift substrate specificity from OPS to OAS. However, none of the active site variants reacted with OAS. An overlay between Y152F/S185G SbnA and an OASS homologue, CysM from *S. typhimurium* (PDB ID: 2JC3) revealed minor structural differences surrounding the PLP cofactor.[27] Therefore, substrate specificity appears to require some other factor in addition to the active sites residues Arg132, Tyr152, and Ser185.

A multiple sequence alignment of SbnA homologues revealed that all three residues identified as unique for OPS binding (Arg132, Tyr152, and Ser185) are conserved in enzymes from putative L-Dap biosynthesis pathways. In addition, examples of OPSS enzymes not involved in L-Dap biosynthesis are known: CysM[45,57] and CysK2[58] from *M. tuberculosis* and CysO[28] from *Aeropyrum pernix* K1. OPS is the preferred substrate of both CysM and CysO, but unlike SbnA, they are also capable of reacting with OAS to generate the PLP-α-aminoacrylate intermediate.[45] CysK2 behaves more like SbnA, with specificity for OPS alone.[58] The CysM and CysO crystal structures have comparable active sites to SbnA except that SbnA is missing a loop that lies directly above the PLP cofactor. This loop contains a conserved arginine that is important for OPS specificity over OAS in CysM.[57] The analogous arginine is missing from SbnA, but Arg132 is located on the opposite side of the active site pocket and is essential for OPS activity, suggesting it fulfills a similar role. Additionally, CysO lacks the conserved Tyr152 present in SbnA, CysM, and CysK2, which is replaced with a phenylalanine residue.[59,60] A CysO variant K127A crystal structure complexed with OPS revealed that the OPS phosphoryl group had limited interactions with active site residues, though selectivity may not be an issue for CysO, since *A. pernix* is not predicted to synthesize OAS as genome sequence analyses failed to identify a serine acetyltransferase that catalyzes the formation of OAS from L-serine and acetyl-CoA. Furthermore, *A. pernix* is a hyperthermophile living in temperatures between 90 and 95 °C where OAS is labile at high temperatures, while OPS is heat stable.[28] Therefore, the requirement of a tyrosine residue in CysO to improve substrate specificity may not be essential given its unique environment.

In SbnA-AA, a citrate molecule was identified bound above the PLP-α-aminoacrylate. Since citrate is not a substrate for SbnA and is structurally similar to L-glutamate, we hypothesize that L-glutamate binds at this site with the nitrogen poised to attack the β-carbon of the α-aminoacrylate. Attempts to cocrystallize or soak L-glutamate into SbnA-OPS crystals were unsuccessful. The high concentration of citrate present in the crystallization solution (~1.0 M) likely outcompetes L-glutamate for binding into the second substrate binding pocket. Inspection of citrate bound to SbnA suggests that L-glutamate binding is likely mediated by three conserved positively charged residues: Lys100, Arg132, and Arg224. Also, the multiple sequence alignment revealed a four amino acid insertion ($G_{126}G_{127}Y_{128}L_{129}$) preceding Arg132 that are modestly conserved in SbnA and homologues that are implicated in L-Dap biosynthesis, but not present in other OASS or OPSS enzymes (Figure 3A). Tyr128 and Leu129 mainchain atoms form hydrogen bonds with citrate in the SbnA-AA (Figure 2E). The Tyr128 side chain formed two CH/π interactions to Pro99 and Pro122 in both the open and closed conformations. Additionally, the Leu129 side chain forms part of the citrate-

DOI: 10.1021/acs.biochem.5b01045
Biochemistry 2016, 55, 927−939

binding pocket in the SbnA-AA. The location and conservation of these residues support a role of this pocket in determining the specificity of SbnA for L-glutamate.

Formation of the PLP-α-aminoacrylate intermediate in SbnA is competitively inhibited by L-cysteine. Typically, L-cysteine is generated as the product from OASS and OPSS enzymes.[25,57] On the basis of the KEGG database, an analysis of amino acid biosynthetic pathways in *S. aureus* revealed a direct link between L-Dap and L-cysteine.[54,55] L-Cysteine is ultimately derived from the glycolytic intermediate 3-phosphoglycerate (Figure 6). To produce L-cysteine, OPS is dephosphorylated to produce L-serine by phosphoserine phosphatase (SerB). Next, L-serine is acetylated by a serine acetyltransferase (CysE) and then converted to L-cysteine by cysteine synthase (CysK). Therefore, L-Dap, L-serine, and L-cysteine are all derived from OPS. Thus, inhibition of SbnA by L-cysteine would reduce OPS consumption and favor the production of L-serine and other downstream products.

Inhibiting SbnA activity with L-cysteine may be another example of coordination between iron homeostasis and oxidative stress response in *S. aureus*.[61,62] In this model, L-cysteine may play a role in regulating iron homeostasis by limiting the production of SB and ultimately iron uptake to decrease the generation of the more damaging reactive oxygen species from H_2O_2 via the Fenton reaction (Figure 6).[63] In *S. aureus*, sulfur homeostasis is controlled by the repressor CymR.[64] Repression is mediated by CymR when in complex with CysK and is alleviated upon OAS binding to CysK.[64] In addition to sulfur metabolism, CymR also plays a role in the oxidative stress response by indirectly regulating genes such as *copA*, *ahpC*, *soda*, *ftnA*, and *dps*.[65] More recently, CymR was also identified to act as an oxidation-sensing regulator where its sole cysteine thiol is oxidized to sulfenic acid upon exposure to H_2O_2, resulting in the loss of DNA binding.[66] The consequence of losing CymR regulation results in an ~68-fold increase in the intracellular L-cysteine concentration in a Δ*cymR S. aureus* mutant compared to the parental strain.[65] Therefore, under oxidative stress, the increased production of L-cysteine concentration, via CymR regulation, would create a more reducing intracellular environment (Figure 6). L-Cysteine itself is incorporated into thiol redox enzymes (e.g., thioredoxin reductase and thioredoxin) and is a key constituent of bacillithiol, a low-molecular weight thiol that is crucial in fomycin resistance.[67] The increased concentration of L-cysteine in *S. aureus* would limit the production of L-Dap by inhibiting SbnA activity, thus reducing iron uptake by the SB pathway and limiting the production of damaging reactive oxygen species (Figure 6).

In summary, we have provided insight into how SbnA mediates substrate specificity for OPS and L-glutamate. For OPS specificity, three active site residues Arg132, Try152, and Ser185 were shown to be essential for OPS recognition and turnover. In the structure of the PLP-α-aminoacrylate intermediate of SbnA, a second substrate-binding pocket occupied by citrate was observed directly above the PLP-α-aminoacrylate. The citrate binding site is suggested to also bind L-glutamate. Furthermore, L-cysteine was identified as a competitive inhibitor of SbnA by forming a nonproductive external aldimine complex with PLP. L-Cysteine inhibition of SbnA is proposed to link the SB biosynthetic pathway to the oxidative stress response in *S. aureus* to reduce iron uptake under oxidative stress.

■ ASSOCIATED CONTENT

Supporting Information

The Supporting Information is available free of charge on the ACS Publications website at DOI: 10.1021/acs.biochem.5b01045.

A list of phosphorylated mutagenic primers used to generate SbnA variants (Table S1), molecular weight determination of SbnA using size exclusion chromatography multiangular lightscattering (Figure S1), UV−visible absorption spectra of wild type, S185G SbnA, Y152F/S185G SbnA, and R132A SbnA (Figure S2), NADH enzyme coupled assay for the production of ACEGA from wild type SbnA and variants (Figure S3), the optimization of SbnA activity using different pH ranges and salt concentrations (Figure S4), the Michaelis−Menten plots of wild type SbnA and S185G SbnA using OPS and L-glutamate (Figure S5), the single turnover kinetic plots that show the formation of the PLP-α-aminoacrylate for wild type SbnA, S185G SbnA, and Y152F SbnA using OPS (Figure S6), the structural overlay of wild type SbnA and Y152F SbnA (Figure S7), UV−visible absorption spectra of PLP mixed with L-cysteine (Figure S8), the Michaelis−Menten plots of wild type SbnA and S185G SbnA with varying concentrations of L-cysteine (Figure S9), and the single turnover plots that show the decay of the internal Schiff base for wild type SbnA, S185G SbnA, Y152F SbnA, Y152F/S185G SbnA, and R132A SbnA using L-cysteine (Figure S10) (PDF)

■ AUTHOR INFORMATION

Corresponding Author

*Phone: (604) 822-8022. Fax: (604) 822-6041. E-mail: Michael.Murphy@ubc.ca.

Funding

The research is supported by the Canadian Institutes of Health Research grant MOP-102596. Instrument support was provided by the Canada Foundation for Innovation and the British Columbia Knowledge Development Fund.

Notes

The authors declare no competing financial interest.

■ ACKNOWLEDGMENTS

Research described in this paper was performed using beamline 08B1-1 at the Canadian Light Source, which is supported by the Natural Sciences and Engineering Research Council of Canada, the National Research Council Canada, the Canadian Institutes of Health Research, the Province of Saskatchewan, Western Economic Diversification Canada, and the University of Saskatchewan. Portions of this research were carried out at the Stanford Synchrotron Radiation Lightsource, a Directorate of SLAC National Accelerator Laboratory and an Office of Science User Facility operated for the U.S. Department of Energy Office of Science by Stanford University. The SSRL Structural Molecular Biology Program is supported by the DOE Office of Biological and Environmental Research, and by the National Institutes of Health, National Institute of General Medical Sciences (including P41GM103393). The contents of this publication are solely the responsibility of the authors and do not necessarily represent the official views of NIGMS or NIH. We would like to thank Angelé Arrieta for technical

DOI: 10.1021/acs.biochem.5b01045
Biochemistry 2016, 55, 927−939

assistance. We would also like to thank Dr. Lindsay Eltis and Dr. Rahul Singh for helpful advice and assistance with the stopped-flow kinetics and access to spectrophotometers.

■ ABBREVIATIONS

L-DAP, L-2,3-diaminopropionic acid; OPS, *O*-phospho-L-serine; OAS, *O*-acetyl-L-serine; PLP, pyridoxal 5′-phosphate; SA, Staphyloferrin A; SB, Staphyloferrin B; ACEGA, *N*-(1-amino-1-carboxy-2-ethyl)-glutamic acid; OASS, *O*-acetyl-L-serine sulfhydrylases; OPSS, *O*-phospho-L-serine sulfhydrylase; TCEP, Tris(2-carboxyethyl)phosphine; PLP-AA, SbnA PLP-α-aminoacrylate

■ REFERENCES

(1) Wandersman, C., and Delepelaire, P. (2004) Bacterial iron sources: from siderophores to hemophores. *Annu. Rev. Microbiol. 58*, 611−647.

(2) Sheftel, A. D., Mason, A. B., and Ponka, P. (2012) The long history of iron in the Universe and in health and disease. *Biochim. Biophys. Acta, Gen. Subj. 1820*, 161−187.

(3) Weinberg, E. D. (1974) Iron and susceptibility to infectious disease. *Science 184*, 952−956.

(4) Hammer, N. D., and Skaar, E. P. (2011) Molecular mechanisms of Staphylococcus aureus iron acquisition. *Annu. Rev. Microbiol. 65*, 129−147.

(5) Sheldon, J. R., and Heinrichs, D. E. (2015) Recent developments in understanding the iron acquisition strategies of gram positive pathogens. *FEMS Microbiol Rev. 39*, 592−630.

(6) Konetschny-Rapp, S., Jung, G., Meiwes, J., and Zahner, H. (1990) Staphyloferrin A: a structurally new siderophore from staphylococci. *Eur. J. Biochem. 191*, 65−74.

(7) Drechsel, H., Freund, S., Nicholson, G., Haag, H., Jung, O., Zahner, H., and Jung, G. (1993) Purification and chemical characterization of staphyloferrin B, a hydrophilic siderophore from staphylococci. *BioMetals 6*, 185−192.

(8) Cotton, J. L., Tao, J., and Balibar, C. J. (2009) Identification and characterization of the Staphylococcus aureus gene cluster coding for staphyloferrin A. *Biochemistry 48*, 1025−1035.

(9) Beasley, F. C., Vines, E. D., Grigg, J. C., Zheng, Q., Liu, S., Lajoie, G. A., Murphy, M. E., and Heinrichs, D. E. (2009) Characterization of staphyloferrin A biosynthetic and transport mutants in Staphylococcus aureus. *Mol. Microbiol. 72*, 947−963.

(10) Cheung, J., Beasley, F. C., Liu, S., Lajoie, G. A., and Heinrichs, D. E. (2009) Molecular characterization of staphyloferrin B biosynthesis in Staphylococcus aureus. *Mol. Microbiol. 74*, 594−608.

(11) Dale, S. E., Doherty-Kirby, A., Lajoie, G., and Heinrichs, D. E. (2004) Role of siderophore biosynthesis in virulence of Staphylococcus aureus: identification and characterization of genes involved in production of a siderophore. *Infect. Immun. 72*, 29−37.

(12) Beasley, F. C., Marolda, C. L., Cheung, J., Buac, S., and Heinrichs, D. E. (2011) Staphylococcus aureus transporters Hts, Sir, and Sst capture iron liberated from human transferrin by Staphyloferrin A, Staphyloferrin B, and catecholamine stress hormones, respectively, and contribute to virulence. *Infect. Immun. 79*, 2345−2355.

(13) Hanses, F., Roux, C., Dunman, P. M., Salzberger, B., and Lee, J. C. (2014) Staphylococcus aureus gene expression in a rat model of infective endocarditis. *Genome Med. 6*, 93.

(14) Cheung, J., Murphy, M. E., and Heinrichs, D. E. (2012) Discovery of an iron-regulated citrate synthase in Staphylococcus aureus. *Chem. Biol. 19*, 1568−1578.

(15) Kobylarz, M. J., Grigg, J. C., Sheldon, J. R., Heinrichs, D. E., and Murphy, M. E. (2014) SbnG, a Citrate Synthase in Staphylococcus aureus: A NEW FOLD ON AN OLD ENZYME. *J. Biol. Chem. 289*, 33797−33807.

(16) Beasley, F. C., Cheung, J., and Heinrichs, D. E. (2011) Mutation of L-2,3-diaminopropionic acid synthase genes blocks staphyloferrin B synthesis in Staphylococcus aureus. *BMC Microbiol. 11*, 199.

(17) Kobylarz, M. J., Grigg, J. C., Takayama, S. J., Rai, D. K., Heinrichs, D. E., and Murphy, M. E. (2014) Synthesis of L-2,3-diaminopropionic acid, a siderophore and antibiotic precursor. *Chem. Biol. 21*, 379−388.

(18) Malachowa, N., Whitney, A. R., Kobayashi, S. D., Sturdevant, D. E., Kennedy, A. D., Braughton, K. R., Shabb, D. W., Diep, B. A., Chambers, H. F., Otto, M., and DeLeo, F. R. (2011) Global changes in Staphylococcus aureus gene expression in human blood. *PLoS One 6*, e18617.

(19) Zhao, C., Song, C., Luo, Y., Yu, Z., and Sun, M. (2008) L-2,3-diaminopropionate: one of the building blocks for the biosynthesis of Zwittermicin A in Bacillus thuringiensis subsp. kurstaki strain YBT-1520. *FEBS Lett. 582*, 3125−3131.

(20) Thomas, M. G., Chan, Y. A., and Ozanick, S. G. (2003) Deciphering tuberactinomycin biosynthesis: isolation, sequencing, and annotation of the viomycin biosynthetic gene cluster. *Antimicrob. Agents Chemother. 47*, 2823−2830.

(21) Felnagle, E. A., Rondon, M. R., Berti, A. D., Crosby, H. A., and Thomas, M. G. (2007) Identification of the biosynthetic gene cluster and an additional gene for resistance to the antituberculosis drug capreomycin. *Appl. Environ. Microb 73*, 4162−4170.

(22) Dawlaty, J., Zhang, X., Fischbach, M. A., and Clardy, J. (2010) Dapdiamides, tripeptide antibiotics formed by unconventional amide ligases. *J. Nat. Prod. 73*, 441−446.

(23) Cook, P. F., and Wedding, R. T. (1976) A reaction mechanism from steady state kinetic studies for O-acetylserine sulfhydrylase from Salmonella typhimurium LT-2. *J. Biol. Chem. 251*, 2023−2029.

(24) Kredich, N. M., and Tomkins, G. M. (1966) The enzymic synthesis of L-cysteine in Escherichia coli and Salmonella typhimurium. *J. Biol. Chem. 241*, 4955−4965.

(25) Schnell, R., Oehlmann, W., Singh, M., and Schneider, G. (2007) Structural insights into catalysis and inhibition of O-acetylserine sulfhydrylase from Mycobacterium tuberculosis. Crystal structures of the enzyme alpha-aminoacrylate intermediate and an enzyme-inhibitor complex. *J. Biol. Chem. 282*, 23473−23481.

(26) Schnackerz, K. D., Tai, C. H., Simmons, J. W., Jacobson, T. M., Rao, G. S. J., and Cook, P. F. (1995) Identification and Spectral Characterization of the External Aldimine of the O-Acetylserine Sulfhydrylase Reaction. *Biochemistry 34*, 12152−12160.

(27) Chattopadhyay, A., Meier, M., Ivaninskii, S., Burkhard, P., Speroni, F., Campanini, B., Bettati, S., Mozzarelli, A., Rabeh, W. M., Li, L., and Cook, P. F. (2007) Structure, mechanism, and conformational dynamics of O-acetylserine sulfhydrylase from Salmonella typhimurium: comparison of A and B isozymes. *Biochemistry 46*, 8315−8330.

(28) Mino, K., and Ishikawa, K. (2003) A novel O-phospho-L-serine sulfhydrylation reaction catalyzed by O-acetylserine sulfhydrylase from Aeropyrum pernix K1. *FEBS Lett. 551*, 133−138.

(29) Hames, C., Halbedel, S., Schilling, O., and Stulke, J. (2005) Multiple-mutation reaction: a method for simultaneous introduction of multiple mutations into the glpK gene of Mycoplasma pneumoniae. *Appl. Environ. Microbiol. 71*, 4097−4100.

(30) Otwinowski, Z., and Minor, W. (1997) Processing of X-ray diffraction data collected in oscillation mode. *Methods Enzymol. 276*, 307−326.

(31) Bunkoczi, G., and Read, R. J. (2011) Improvement of molecular-replacement models with Sculptor. *Acta Crystallogr., Sect. D: Biol. Crystallogr. 67*, 303−312.

(32) Adams, P. D., Afonine, P. V., Bunkoczi, G., Chen, V. B., Davis, I. W., Echols, N., Headd, J. J., Hung, L. W., Kapral, G. J., Grosse-Kunstleve, R. W., McCoy, A. J., Moriarty, N. W., Oeffner, R., Read, R. J., Richardson, D. C., Richardson, J. S., Terwilliger, T. C., and Zwart, P. H. (2010) PHENIX: a comprehensive Python-based system for macromolecular structure solution. *Acta Crystallogr., Sect. D: Biol. Crystallogr. 66*, 213−221.

DOI: 10.1021/acs.biochem.5b01045
Biochemistry 2016, 55, 927−939

(33) McCoy, A. J., Grosse-Kunstleve, R. W., Adams, P. D., Winn, M. D., Storoni, L. C., and Read, R. J. (2007) Phaser crystallographic software. *J. Appl. Crystallogr. 40*, 658−674.
(34) Terwilliger, T. C., Grosse-Kunstleve, R. W., Afonine, P. V., Moriarty, N. W., Zwart, P. H., Hung, L. W., Read, R. J., and Adams, P. D. (2008) Iterative model building, structure refinement and density modification with the PHENIX AutoBuild wizard. *Acta Crystallogr., Sect. D: Biol. Crystallogr. 64*, 61−69.
(35) Emsley, P., Lohkamp, B., Scott, W. G., and Cowtan, K. (2010) Features and development of Coot. *Acta Crystallogr., Sect. D: Biol. Crystallogr. 66*, 486−501.
(36) Murshudov, G. N., Vagin, A. A., and Dodson, E. J. (1997) Refinement of macromolecular structures by the maximum-likelihood method. *Acta Crystallogr., Sect. D: Biol. Crystallogr. 53*, 240−255.
(37) Winn, M. D., Ballard, C. C., Cowtan, K. D., Dodson, E. J., Emsley, P., Evans, P. R., Keegan, R. M., Krissinel, E. B., Leslie, A. G. W., McCoy, A., McNicholas, S. J., Murshudov, G. N., Pannu, N. S., Potterton, E. A., Powell, H. R., Read, R. J., Vagin, A., and Wilson, K. S. (2011) Overview of the CCP4 suite and current developments. *Acta Crystallogr., Sect. D: Biol. Crystallogr. 67*, 235−242.
(38) Kabsch, W. (2010)) Xds. *Acta Crystallogr., Sect. D: Biol. Crystallogr. 66*, 125−132.
(39) Kabsch, W. (2010) Integration, scaling, space-group assignment and post-refinement. *Acta Crystallogr., Sect. D: Biol. Crystallogr. 66*, 133−144.
(40) Leslie, A. G. W., and Powell, H. R. (2007) Processing diffraction data with MOSFLM. *Nato Sci. Ser. II Math 245*, 41−51.
(41) Evans, P. (2006) Scaling and assessment of data quality. *Acta Crystallogr., Sect. D: Biol. Crystallogr. 62*, 72−82.
(42) Afonine, P. V., Grosse-Kunstleve, R. W., Echols, N., Headd, J. J., Moriarty, N. W., Mustyakimov, M., Terwilliger, T. C., Urzhumtsev, A., Zwart, P. H., and Adams, P. D. (2012) Towards automated crystallographic structure refinement with phenix.refine. *Acta Crystallogr., Sect. D: Biol. Crystallogr. 68*, 352−367.
(43) Painter, J., and Merritt, E. A. (2006) Optimal description of a protein structure in terms of multiple groups undergoing TLS motion. *Acta Crystallogr., Sect. D: Biol. Crystallogr. 62*, 439−450.
(44) Webb, M. R. (1992) A continuous spectrophotometric assay for inorganic phosphate and for measuring phosphate release kinetics in biological systems. *Proc. Natl. Acad. Sci. U. S. A. 89*, 4884−4887.
(45) O'Leary, S. E., Jurgenson, C. T., Ealick, S. E., and Begley, T. P. (2008) O-phospho-L-serine and the thiocarboxylated sulfur carrier protein CysO-COSH are substrates for CysM, a cysteine synthase from Mycobacterium tuberculosis. *Biochemistry 47*, 11606−11615.
(46) Sievers, F., Wilm, A., Dineen, D., Gibson, T. J., Karplus, K., Li, W., Lopez, R., McWilliam, H., Remmert, M., Soding, J., Thompson, J. D., and Higgins, D. G. (2011) Fast, scalable generation of high-quality protein multiple sequence alignments using Clustal Omega. *Mol. Syst. Biol. 7*, 539.
(47) Eliot, A. C., and Kirsch, J. F. (2004) Pyridoxal phosphate enzymes: mechanistic, structural, and evolutionary considerations. *Annu. Rev. Biochem. 73*, 383−415.
(48) Krissinel, E., and Henrick, K. (2007) Inference of macromolecular assemblies from crystalline state. *J. Mol. Biol. 372*, 774−797.
(49) Ro, H. S. (2002) Effects of salts on the conformation and catalytic properties of d-amino acid aminotransferase. *J. Biochem. Mol. Biol. 35*, 306−312.
(50) Shibata, K., Shirasuna, K., Motegi, K., Kera, Y., Abe, H., and Yamada, R. (2000) Purification and properties of alanine racemase from crayfish Procambarus clarkii. *Comp. Biochem. Physiol., Part B: Biochem. Mol. Biol. 126*, 599−608.
(51) Matsuo, Y. (1957) Formation of Schiff Bases of Pyridoxal Phosphate - Reaction with Metal Ions. *J. Am. Chem. Soc. 79*, 2011−2015.
(52) Townsend, D. E., Kaenjak, A., Jayaswal, R. K., and Wilkinson, B. J. (1996) Proline is biosynthesized from arginine in Staphylococcus aureus. *Microbiology 142*, 1491−1497.
(53) Liebeke, M., Dorries, K., Zuhlke, D., Bernhardt, J., Fuchs, S., Pane-Farre, J., Engelmann, S., Volker, U., Bode, R., Dandekar, T., Lindequist, U., Hecker, M., and Lalk, M. (2011) A metabolomics and proteomics study of the adaptation of Staphylococcus aureus to glucose starvation. *Mol. BioSyst. 7*, 1241−1253.
(54) Kanehisa, M., Goto, S., Sato, Y., Kawashima, M., Furumichi, M., and Tanabe, M. (2014) Data, information, knowledge and principle: back to metabolism in KEGG. *Nucleic Acids Res. 42*, D199−205.
(55) Kanehisa, M., and Goto, S. (2000) KEGG: kyoto encyclopedia of genes and genomes. *Nucleic Acids Res. 28*, 27−30.
(56) Agren, D., Schnell, R., and Schneider, G. (2009) The C-terminal of CysM from Mycobacterium tuberculosis protects the aminoacrylate intermediate and is involved in sulfur donor selectivity. *FEBS Lett. 583*, 330−336.
(57) Agren, D., Schnell, R., Oehlmann, W., Singh, M., and Schneider, G. (2008) Cysteine synthase (CysM) of Mycobacterium tuberculosis is an O-phosphoserine sulfhydrylase: evidence for an alternative cysteine biosynthesis pathway in mycobacteria. *J. Biol. Chem. 283*, 31567−31574.
(58) Steiner, E. M., Both, D., Lossl, P., Vilaplana, F., Schnell, R., and Schneider, G. (2014) CysK2 from Mycobacterium tuberculosis is an O-phospho-L-serine-dependent S-sulfocysteine synthase. *J. Bacteriol. 196*, 3410−3420.
(59) Nakamura, T., Kawai, Y., Kunimoto, K., Iwasaki, Y., Nishii, K., Kataoka, M., and Ishikawa, K. (2012) Structural analysis of the substrate recognition mechanism in O-phosphoserine sulfhydrylase from the hyperthermophilic archaeon Aeropyrum pernix K1. *J. Mol. Biol. 422*, 33−44.
(60) Oda, Y., Mino, K., Ishikawa, K., and Ataka, M. (2005) Three-dimensional structure of a new enzyme, O-phosphoserine sulfhydrylase, involved in l-cysteine biosynthesis by a hyperthermophilic archaeon, Aeropyrum pernix K1, at 2.0A resolution. *J. Mol. Biol. 351*, 334−344.
(61) Horsburgh, M. J., Ingham, E., and Foster, S. J. (2001) In *Staphylococcus aureus*, fur is an interactive regulator with PerR, contributes to virulence, and Is necessary for oxidative stress resistance through positive regulation of catalase and iron homeostasis. *J. Bacteriol. 183*, 468−475.
(62) Horsburgh, M. J., Clements, M. O., Crossley, H., Ingham, E., and Foster, S. J. (2001) PerR controls oxidative stress resistance and iron storage proteins and is required for virulence in *Staphylococcus aureus*. *Infect. Immun. 69*, 3744−3754.
(63) Park, S., and Imlay, J. A. (2003) High levels of intracellular cysteine promote oxidative DNA damage by driving the fenton reaction. *J. Bacteriol. 185*, 1942−1950.
(64) Soutourina, O., Poupel, O., Coppee, J. Y., Danchin, A., Msadek, T., and Martin-Verstraete, I. (2009) CymR, the master regulator of cysteine metabolism in Staphylococcus aureus, controls host sulphur source utilization and plays a role in biofilm formation. *Mol. Microbiol. 73*, 194−211.
(65) Soutourina, O., Dubrac, S., Poupel, O., Msadek, T., and Martin-Verstraete, I. (2010) The pleiotropic CymR regulator of *Staphylococcus aureus* plays an important role in virulence and stress response. *PLoS Pathog. 6*, e1000894.
(66) Ji, Q. J., Zhang, L., Sun, F., Deng, X., Liang, H. H., Bae, T. O., and He, C. (2012) Staphylococcus aureus CymR Is a New Thiol-based Oxidation-sensing Regulator of Stress Resistance and Oxidative Response. *J. Biol. Chem. 287*, 21102−21109.
(67) Posada, A. C., Kolar, S. L., Dusi, R. G., Francois, P., Roberts, A. A., Hamilton, C. J., Liu, G. Y., and Cheung, A. (2014) Importance of bacillithiol in the oxidative stress response of *Staphylococcus aureus*. *Infect. Immun. 82*, 316−332.

DOI: 10.1021/acs.biochem.5b01045
Biochemistry 2016, 55, 927−939